Available online at www.sciencedirect.com

ScienceDirect

www.elsevier.com/locate/jes

JES JOURNAL OF ENVIRONMENTAL SCIENCES

www.jesc.ac.cn

Effects of Na^+ on Cu/SAPO-34 for ammonia selective catalytic reduction

Can Wang[1], Chen Wang[2], Jun Wang[1], Jianqiang Wang[1], Meiqing Shen[1,3,4,], Wei Li[5,*]*

1. *Key Laboratory for Green Chemical Technology of State Education Ministry, School of Chemical Engineering & Technology, Tianjin University, Tianjin 300350, China. E-mail:* canwang@tju.edu.cn
2. *School of Environment and Safety Engineering, North University of China, Taiyuan 030051, China*
3. *Collaborative Innovation Centre of Chemical Science and Engineering (Tianjin), Tianjin 300350, China*
4. *State Key Laboratory of Engines, Tianjin University, Tianjin 300350, China*
5. *General Motors Global Research and Development, Chemical Sciences and Materials Systems Lab, 30500 Mound Road, Warren, MI 48090, USA*

ARTICLE INFO

Article history:
Received 24 July 2017
Revised 31 October 2017
Accepted 2 November 2017
Available online 14 November 2017

Keywords:
Cu/SAPO-34
Ammonia selective catalytic reduction (NH_3-SCR)
Na effects
Ion-exchange

ABSTRACT

Copper-exchanged chabazite (Cu/CHA) catalysts have been found to be affected by alkali metal and alkaline earth ions. However, the effects of Na^+ ions on Cu/SAPO-34 for ammonia selective catalytic reduction (NH_3-SCR) are still unclear. In order to investigate the mechanism, five samples with various Na contents were synthesized and characterized. It was observed that the introduced Na^+ ion-exchanges with H^+ and Cu^{2+} of Cu/SAPO-34. The exchange of H^+ is easier than that of isolated Cu^{2+}. The exchanged Cu^{2+} ions aggregate and form "$CuAl_2O_4$-like" species. The NH_3-SCR activity of Cu/SAPO-34 decreases with increasing Na content, and the loss of isolated Cu^{2+} and acid sites is responsible for the activity loss.

Introduction

Ammonia selective catalytic reduction (NH_3-SCR) has been considered to be one of the most promising techniques to reduce NO_x emissions due to its high efficiency and broad operating temperature window (Koebel et al., 2000). Copper chabazites (Cu/CHA, *e.g.*, Cu/SSZ-13 and Cu/SAPO-34) have been studied extensively as excellent SCR catalysts due to their outstanding catalytic activity, N_2 selectivity and hydrothermal stability (Fickel et al., 2011; Ishihara et al., 1997; Wang et al., 2012, 2013; Xue et al., 2013; Yu et al., 2013; Liu et al., 2016; Ma et al., 2016; Panahi et al., 2015). In spite of their excellent performance in NH_3-SCR, Cu/CHA catalysts face chemical deactivation problems such as sulfur poisoning (Li et al., 2014; Shen et al., 2015) and alkali metal poisoning (Ma et al., 2015; Liu et al., 2015; Xie et al., 2015).

In commercial applications, the ammonia used in NH_3-SCR is produced *via* decomposition of a urea solution that may contain trace amounts of alkali metal and alkaline earth ions (*e.g.*, K^+, Na^+, Ca^{2+}, Mg^{2+}). These ions, which have easy access to the SCR catalyst, have been reported to affect the properties of Cu/CHA catalysts (Fedeyko and Chen, 2015; Gao et al., 2015b; Ma et al., 2015; Liu et al., 2015; Xie et al., 2015). Xie et al. (2015) studied the effects of Na co-cations on the hydrothermal stability of Cu/SSZ-13, and the results showed that Cu/SSZ-13 with high Na contents and low Cu contents exhibited poor

* *Corresponding authors. E-mails:* mqshen@tju.edu.cn (Meiqing Shen), wei.1.li@gm.com (Wei Li).

https://doi.org/10.1016/j.jes.2017.11.002

hydrothermal stability. Fedeyko and Chen (2015) and Gao et al. (2015b) investigated the effects of alkali metal and alkaline earth co-cations (Li^+, Na^+, K^+, Cs^+, Ca^{2+}, Mg^{2+}) on the activity and hydrothermal stability of Cu/SSZ-13. Their results demonstrated that by removing a portion of the Brønsted acid sites, all co-cations helped to mitigate hydrolysis of the zeolite catalysts during hydrothermal aging. For Cu/SAPO-34, Liu et al. (2015) compared the potassium poisoning phenomena of Cu/SAPO-34 and V_2O_5 (WO_3)/TiO_2 by impregnating KOH solution into these two catalysts. The results demonstrated that potassium indeed had negative effects on the catalytic performance of Cu/SAPO-34, even though the poisoning effect of potassium on Cu/SAPO-34 was less significant compared to that of V_2O_5 (WO_3)/TiO_2. Ma et al. (2015) investigated the potassium poisoning mechanism for Cu/SAPO-34 by impregnating the catalyst with KNO_3 solutions, to obtain five samples with different potassium contents. Their results illustrated that the transformation of isolated Cu^{2+} to square-plane copper oxide clusters arising from the potassium poisoning was considered to be the main reason for the deactivation of the Cu-SAPO-34 catalyst, although the Brønsted acid sites were also decreased. The study only investigated the effect of K^+ on Cu/SAPO-34, but both K^+ and Na^+ co-exist in urea solutions. Thus, it is necessary to examine the Na effect on Cu/SAPO-34 and the mechanism of its effect on SCR reactions.

In this study, different Na contents were investigated (0, 0.3, 0.7, 1.0 and 1.5 wt.%). The compositions of these samples were characterized by inductively coupled plasma and atomic emission spectrometry (ICP-AES), and the effects of Na on the structure and Cu species of Cu/SAO-34 were studied through specific surface area test, X-ray diffraction (XRD), temperature programmed desorption by NH_3 (NH_3-TPD), temperature programmed reduction by hydrogen (H_2-TPR) and electron paramagnetic resonance (EPR). Na species were determined with CO_2 adsorption diffuse reflectance infrared Fourier transform spectroscopy (CO_2-DRIFTS). Catalytic performance tests and kinetic experiments were also conducted to explore the effects of Na^+ on the NH_3-SCR reaction, and to gain insights into the mechanism of its effect.

1. Materials and methods

1.1. Catalyst preparation

Cu/SAPO-34 catalysts were synthesized using a modified "one-pot" method from a gel with a molar composition of: 1.0 Al_2O_3:1.0 P_2O_5:0.6 SiO_2:0.05 CuO:0.05 tetraethylenepentamine (TEPA):2.0 morpholine (MOR):60 H_2O (Fan et al., 2013; Gao et al., 2013; Martínez-Franco et al., 2012). The sources of Al, P, Si and Cu were pseudoboehmite (83.5 wt.% Al_2O_3), orthophosphoric acid (99 wt.% H_3PO_4), LUDOX (40% SiO_2) and copper (II) sulfate pentahydrate ($CuSO_4{\cdot}5H_2O$) respectively. MOR was chosen as the template agent and TEPA as the Cu^{2+} complexing agent. The detailed synthesis procedures were as follows: firstly, the H_3PO_4 and the pseudoboehmite were mixed with distilled water and stirred for 2 hr at room temperature, and the mixture was named Mix1. Silica sol, MOR, TEPA and $CuSO_4{\cdot}5H_2O$ were mixed with distilled water and stirred for 1 hr at room temperature, named Mix2. Mix2 was slowly added into Mix1, stirred for more than 3 hr at room temperature, and then sealed in a 200 mL Teflon-lined stainless-steel pressure vessel and heated at 200°C for 44 hr for crystallization in an oven under autogenic pressure. Subsequently, the sediment was separated from the mother liquid by centrifuging, then successively washed with distilled water and centrifuged more than 3 times. Finally, the zeolite powder was dried at 120°C in an oven for 12 hr.

The Na-containing samples were synthesized by wetness impregnation with sodium nitrate solutions. The impregnated samples were firstly dried at 100°C for 12 hr, calcined in a muffle furnace with air at 650°C for 5 hr, and finally treated at 750°C for 24 hr in 10 vol.% H_2O/air to imitate the interaction environment of Na^+ and Cu/SAPO-34. The Na-free sample was impregnated with pure water and treated like the Na-containing samples. The fresh sample is designated Cu-F, and others are named Cu-NaX, where "X" represents the nominal weight percentage of sodium. The compositions of the samples from ICP measurements are listed in Table 1 and all catalysts contain similar Cu contents with varying amounts of Na.

1.2. Characterization of catalysts

The compositions (Cu and Na contents) of Cu/SAPO-34 catalysts were determined by ICP-AES.

XRD patterns (Cu $K\alpha$ radiation, wavelength (λ) = 1.5418 Å) (Bruker D8 Advance TXS, Bruker, USA) were used to characterize the structure and phase compositions of catalysts, measured in the range of $5° < 2\theta < 50°$ with a step size of 0.01°. Brunauer–Emmett–Teller (BET) surface area was calculated from the linear portion of the BET plot through measuring the N_2 isotherm of the samples at 77 K using F-Sorb 3400 volumetric adsorption–desorption apparatus (F-Sorb 3400, Jin Aipu, China). The catalysts were evacuated at 150°C for 3 hr to remove absorbed water and clean the surface of the catalysts before the measurement.

NH_3-TPD experiments were performed to evaluate the acid sites of the catalysts. 0.1 g catalyst (powder 60–80 mesh) and 0.9 g quartz sand were mixed, and then the mixture was packed in a plug flow reactor. A K type thermocouple was inserted into the center of the catalyst to control the temperature. Prior to the experiments, the catalysts were pretreated at 500°C in 5% O_2/N_2 for 30 min, and then cooled to 100°C. When the temperature had become stable, 500 ppm NH_3/N_2 was flowed through until the outlet NH_3 concentration was stable. Then the catalysts were purged with N_2 to remove weakly absorbed NH_3 until the NH_3 concentration in the outlet gas was lower than 10 ppm. Finally, the catalysts were heated from 100 to 600°C with a ramp rate of

Table 1 – Chemical composition of Cu/SAPO-34 catalysts.

Samples	Cu-F (fresh sample)	Cu-$Na_{0.4}$	Cu-$Na_{0.8}$	Cu-$Na_{1.3}$	Cu-$Na_{1.8}$
Cu contents (wt.%)	1.95	1.95	1.93	2.02	2.04
Na contents (wt.%)	–	0.37	0.80	1.29	1.77

10°C/min. A Fourier transform infrared spectrometer (FTIR) (MKS-2030, MKS Instruments, USA) was used to analyze the outlet NH_3 concentration.

H_2-TPR was performed to identify the reducibility and distribution of Cu species in catalysts. Prior to the experiment, the samples were pretreated at 500°C in 5% O_2/N_2 for 30 min, and then cooled to 30°C; when the temperature achieved stability, 5% H_2/N_2 was flowed through until the bridge current was stable, and the catalysts were elevated at a ramp rate of 10°C/min from 30 to 900°C. The hydrogen consumption was analyzed by a thermal conductivity detector (TCD).

EPR was performed to probe the surrounding environment and quantity the isolated Cu^{2+}. The spectra were acquired on a Bruker ESP A320 spectrometer (ESP A320, Bruker, USA) at −120°C and atmospheric pressure. The Bruker ESP A320 software and a special Bruker program were used for data analysis. For observing the hyperfine splitting of the isolated Cu^{2+} species, the catalysts were treated for 2 hr at 600°C under air to dehydrate them before the experiment.

DRIFTS was performed to study the structural properties of the catalysts, using a FTIR (Nicolet 6700, Thermo Scientific, USA) equipped with a mercury cadmium telluride (MCT) detector at a resolution of 2 cm^{-1}, averaging 32 scans for each spectrum. For *ex-situ* DRIFTS, KBr was chosen as the standard substance to establish the background spectrum. The samples were initially treated in 5% O_2/N_2 at 500°C for 30 min, and then cooled to 150°C under N_2 purging, until the temperature became stable, the spectra were collected. For CO_2-DRIFTS, the samples were initially treated in 5% O_2/N_2 at 500°C for 30 min, and then cooled to 50°C in N_2. The background spectrum was collected first when the temperature became stable, then the sample was purged in 1% CO_2/N_2 for 15 min and N_2 for only 30 min, and the spectra were collected.

1.3. Catalytic performance tests

The NH_3-SCR catalytic performance was tested in a quartz reactor (20 mm inner diameter) at atmospheric pressure, using 0.1 g catalyst (60–80 mesh) with 0.9 g quartz sand (60–80 mesh). The temperature was monitored by a K type thermocouple inserted into the center of the catalyst. The concentrations of NO, NO_2, N_2O and NH_3 were measured by a FTIR spectrometer (MKS-2030, MKS, USA) equipped with a 5.11 m gas cell. The gas hourly space velocity (GHSV) was 720,000 hr^{-1}, and the reaction gas composition was 500 ppm NO, 500 ppm NH_3, 5% O_2, 2% H_2O, 8% CO_2 balanced with N_2. Prior to the tests, the catalysts were heated to 500°C for 30 min under 5% O_2/N_2 with a ramp rate of 10°C/min. When the system was cooled down to 100°C, the reactants were introduced into the reactor. When the outlet concentrations became stable, the catalysts were heated at a ramp rate of 10°C/min from 100 to 600°C. The concentrations of outlet gases were analyzed by a FTIR spectrometer (MKS-2030, MKS, USA). The NO conversion was calculated using the following equation:

$$NO_x \text{ conversion} = \frac{[NO_x]_{inlet} - [NO_x]_{outlet}}{[NO_x]_{inlet}} \times 100\% \quad (1)$$

where $[NO_x]_{inlet}$ represents NO_x concentration before entering reactor, $[NO_x]_{outlet}$ represents NO_x concentration after reacting.

1.4. Kinetic measurements

NH_3-SCR kinetic tests were performed in a thin quartz tube, using 0.025 g catalyst mixed with 0.075 g quartz sand packed in the plug flow reactor. The temperature was controlled by a K type thermocouple inserted into the center of the catalyst bed. Mass flow controllers were used to control the gas composition, and a FTIR spectrometer (MKS-2030, MKS, USA) equipped with a 5.11 m gas cell was used to analyze the outlet gas concentrations. To exclude the influence of internal and external diffusion effects, the total gas flow rate was chosen to be 1.5 L/min (GHSV = 432,000 hr^{-1}) and the particle size was chosen as 80–100 mesh. The specific process is described in detail in Appendix A. Supplementary data. The kinetic test conditions were: 500 ppm NH_3, 500 ppm NO, 5% O_2 balanced by N_2. To control the NO conversion in the kinetic control range, the steady-state kinetic measurements were conducted in the temperature range from 170 to 240°C. The isolated Cu^{2+} ions have been suggested to be the active sites of NH_3-SCR reaction over Cu/SAPO-34 (Xue et al., 2013). Hence, the turnover frequency (TOF) could be calculated from the NO_x conversion by:

$$TOF = \frac{X_{NO_x} \times F_{NO_x} \times 63.5}{60 \times 22.4 \times 100 \times m_{cata} \times M_{Cu^{2+}}} \times 100\% \quad (2)$$

where X_{NOx} (%) is the NO_x conversion, F_{NOx} (L(NO_x)/min) is the flow rate of NO_x, m_{cata} (g) is the mass of catalysts, $M_{Cu^{2+}}$ (%) is the number of isolated Cu^{2+} sites (based on EPR), 63.5 (g/mol) is the molar mass of Cu, and 22.4 (L/mol) is the gas volume in standard condition.

2. Results

2.1. Cu/SAPO-34 structural properties

2.1.1. XRD and BET results

XRD measurements were used to characterize the phase composition and structure of the catalysts. Fig. 1 shows that all catalysts exhibit the typical CHA structure (Prakash and

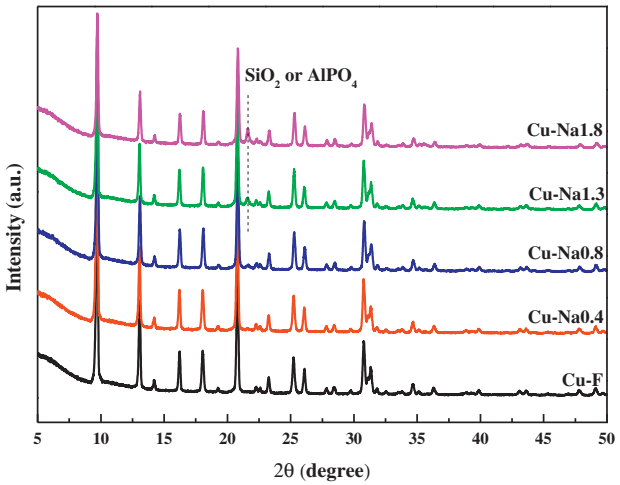

Fig. 1 – X-ray diffraction (XRD) profiles of Cu/SAPO-34 catalysts.

Unnikrishnan, 1994). However, a new diffraction peak at 21.65° assigned to SiO_2 or $AlPO_4$ appeared in Na-containing samples (Wondraczek et al., 2013). This result indicates that structure of Cu/SAPO-34 was damaged slightly. No crystalline diffraction peaks of Na species were detected, suggesting that Na species are highly dispersed. The BET surface areas of these five samples are 577, 547, 523, 469, 464 m^2/g respectively. The BET surface areas of catalysts declined with increasing Na content.

2.1.2. NH_3-TPD results

To identify the density and strength of the acid sites in Cu/SAPO-34, NH_3-TPD measurements were carried out and the results are shown in Fig. 2. All samples show similar desorption curves, with three peaks. The desorption peaks around 180, 230 and 350°C are attributed to NH_3 adsorption on the surface hydroxyl groups (Si–OH, P–OH and Al–OH), weak Brønsted acid sites (Si–OH–Al), and strong Brønsted acid sites (Si–OH–Al) or Lewis acid sites (Si–O(Cu)–Al), respectively (Wang et al., 2015a, 2015b; Yu et al., 2013).

The numbers of acid sites were calculated by integrating the desorption peaks, and the results are listed in Fig. 2b. Notably, the desorption peak at 350°C assigned to strong Brønsted and Lewis acid sites declined as the Na content increased. The results show that the introduction of Na^+ mainly affects the strong Brønsted acid sites (Si–OH–Al) and Lewis acid sites (Si–O(Cu)–Al).

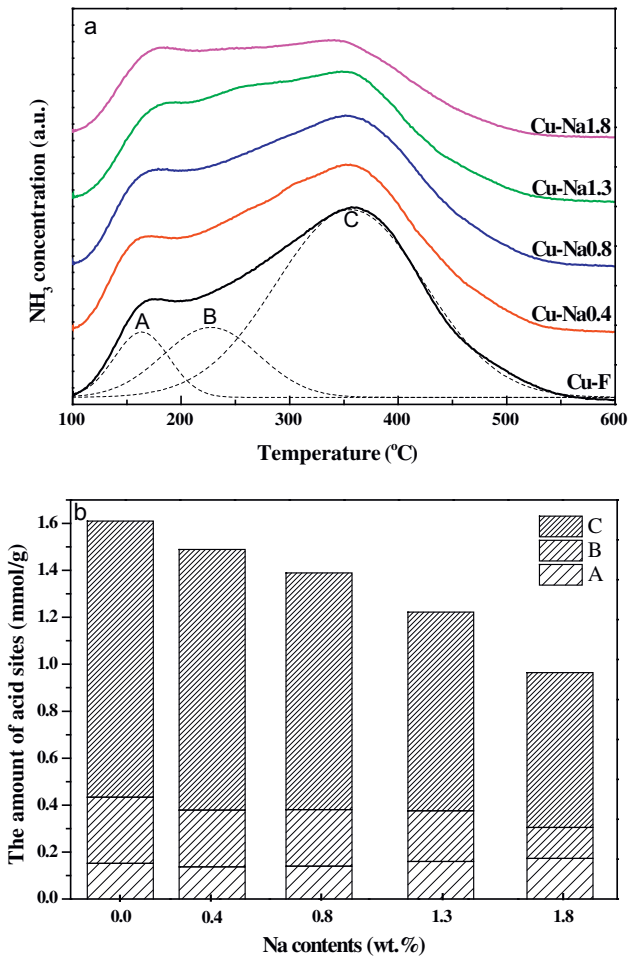

Fig. 2 – (a) Temperature programmed desorption by NH_3 (NH_3-TPD) profiles of Cu/SAPO-34 catalysts; (b) Amount of acid sites based on NH_3-TPD. The desorption peaks around 180, 230 and 350°C are markd as A, B and C, which are attributed to NH_3 adsorption on the surface hydroxyl groups (Si–OH, P–OH and Al–OH), weak Brønsted acid sites (Si–OH–Al), and strong Brønsted acid sites (Si–OH–Al) or Lewis acid sites (Si–O(Cu)–Al), respectively.

2.1.3. CO_2-DRIFTS results

CO_2-DRIFTS were used to monitor the state of Na species (Fig. 3). Compared with Cu–F, two peaks around 2352 and 2345 cm^{-1} appear in the spectra of Na-containing samples. According to the literature (Bonelli et al., 2000; Garrone et al., 2002), the vibrational peak of CO_2 gas molecules is centered at 2349 cm^{-1}. When isolated Na^+ is present in the system, the peak will shift due to the interaction between Na^+ and CO_2. The two peaks are assigned to the vibrations of CO_2 interacting with Si–O (Na^+)–Al. As shown in Fig. 3, the intensities of these two peaks increase with increasing Na content, demonstrating that the Si–O(Na^+)–Al structure forms and in turn, suggesting that Na^+ ion-exchanges with H^+ and Cu^{2+}.

2.2. Distribution of copper species in Cu/SAPO-34

2.2.1. H_2-TPR results

H_2-TPR was carried out on the fresh and Na-containing catalysts, and the results are shown in Fig. 4. The H_2 consumption profile of Cu–F can be divided into three peaks (A, B, D), while Na-containing catalysts present a new peak (C). The peaks of A, B, C and D represent four types of copper species. Usually (Fan et al., 2013; Wang et al., 2014; Xue et al., 2013), peak A is assigned to the reduction of isolated Cu^{2+} to Cu^+, peak B is ascribed to the reduction of CuO to Cu^0 and peak D in the high temperature range is attributed to the reduction of Cu^+ to Cu^0; while the new Peak C is assigned to "$CuAl_2O_4$-like" species (Gao et al., 2015a).

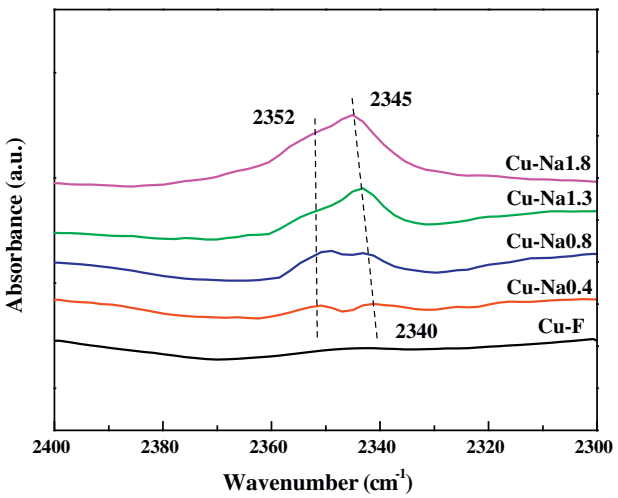

Fig. 3 – Diffuse reflectance infrared Fourier transform spectroscopy (DRIFTS) results of CO_2 adsorbed on Cu/SAPO-34 catalysts.

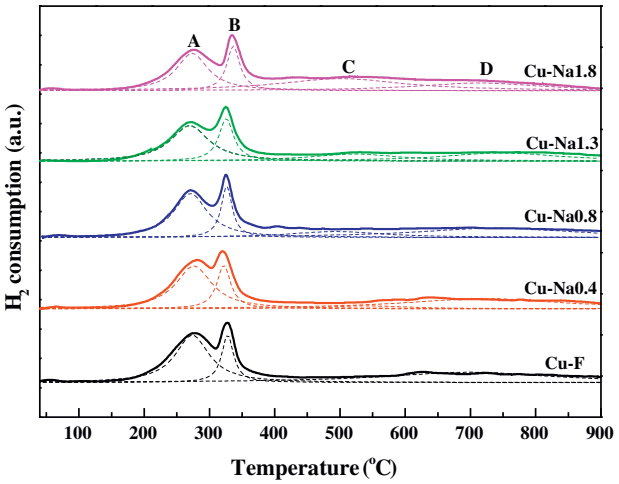

Fig. 4 – Temperature programmed reduction by hydrogen (H_2-TPR) profiles of Cu/SAPO-34 catalysts. The peaks of A, B, C and D represent four types of copper species. Usually, Peak A is assigned to the reduction of isolated Cu^{2+} to Cu^{+}, peak B is ascribed to the reduction of CuO to Cu^0, Peak C is assigned to "$CuAl_2O_4$-like" species and peak D in the high temperature range is attributed to the reduction of Cu^{+} to Cu^0.

Fig. 5 shows that the amount of isolated Cu^{2+} decreases, whereas the amount of "$CuAl_2O_4$-like" species increases as the Na content increases. In addition, the amounts of CuO species remain the same. This reveals that the isolated Cu^{2+} turns into "$CuAl_2O_4$-like" species after Na introduction.

2.2.2. EPR results

EPR was used to probe the coordination environment of isolated Cu^{2+} in the Cu-zeolite catalysts and quantify the amount of isolated Cu^{2+} (Fig. 6a). All catalysts show the same $g_{//} = 2.39$ ($g_{//}$ is the g factor corresponding to the center of the hyperfine splitting of the EPR signal, and is related to the substance type and coordination information. g factor can be calculated by equation: $g = h\upsilon/\beta H$, wherein h is the Planck constant, υ is the frequency of the applied electromagnetic wave, β is the Bohr magnet, and H is the magnetic field strength), indicating the same coordination of isolated Cu^{2+} for samples with or without Na^{+} (Wang et al., 2015a; Xue et al., 2013). A new feature (region b) is found at ~3310 G on Cu-Na1.3 and Cu-Na1.8 (in order to clearly display the feature, the derivative of the EPR signal around 3310 G is shown in Fig. 6b), which can be assigned to the effects of "$CuAl_2O_4$-like" species (Gao et al., 2015a).

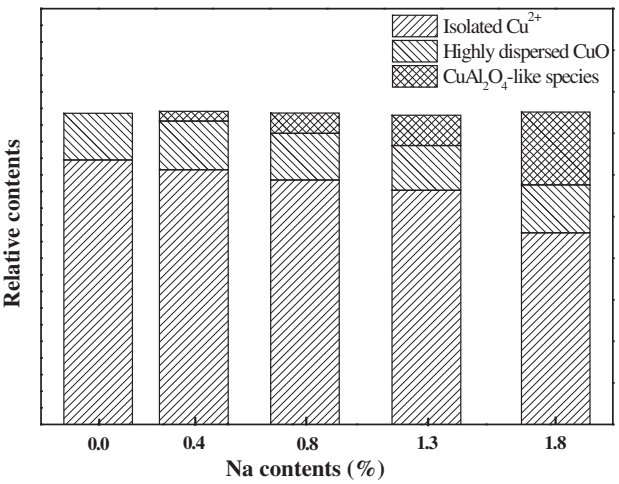

Fig. 5 – Relative amounts of each copper species in Cu/SAPO-34 catalysts based on H_2-TPR.

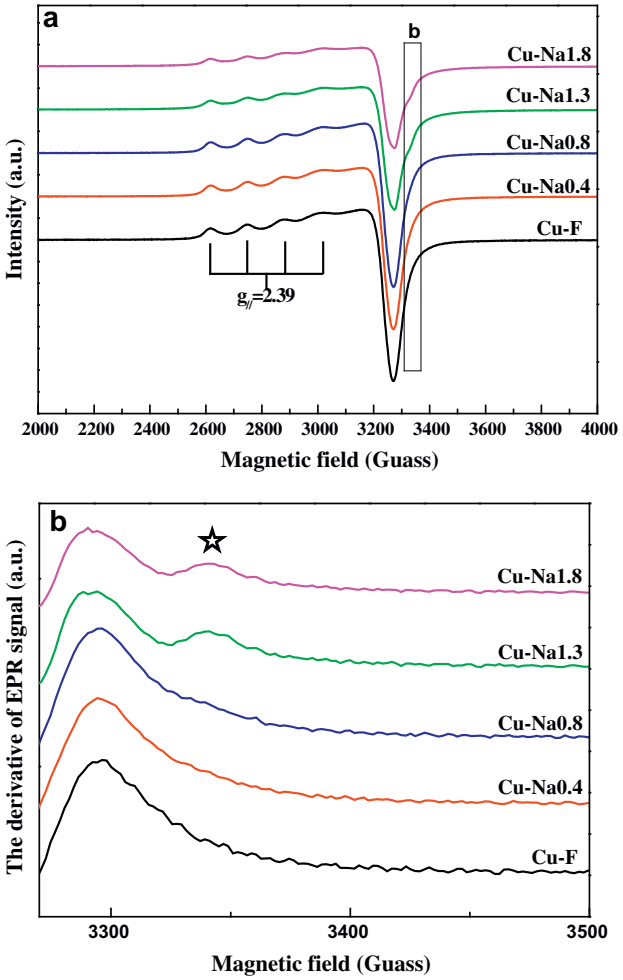

Fig. 6 – Electron paramagnetic resonance (EPR) spectra collected at –120°C of Cu/SAPO-34 catalysts: (a) EPR signal; (b) the derivative of the EPR signal around 3310 G. The star symbol represents the signal change around 3310 G in panel a. $g_{//}$ is the g factor corresponding to the center of the hyperfine splitting of the EPR signal, and is related to the substance type and coordination information. g factor can be calculated by equation: $g = h\upsilon/\beta H$, wherein h is the Planck constant, υ is the frequency of the applied electromagnetic wave, β is the Bohr magnet, and H is the magnetic field strength.

Using $CuSO_4$ solution as the standard substance, the amount of isolated Cu^{2+} ions was estimated by double integration of the signals in Fig. 6a. Fig. 7 shows that the amount of isolated Cu^{2+} declines with increasing Na content, which is consistent with the results of H_2-TPR.

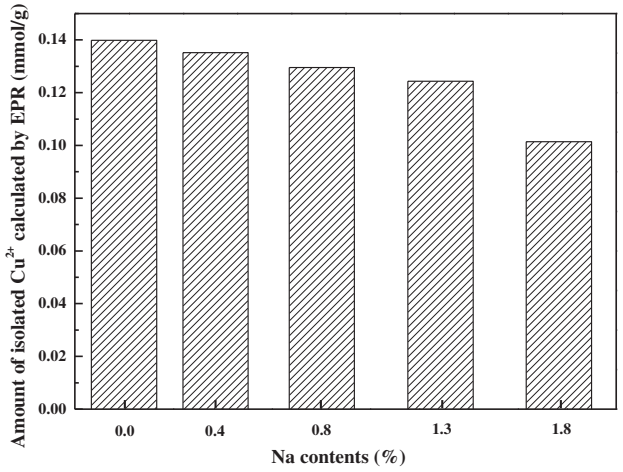

Fig. 7 – Amount of isolated Cu^{2+} of Cu/SAPO-34 catalysts calculated based on EPR.

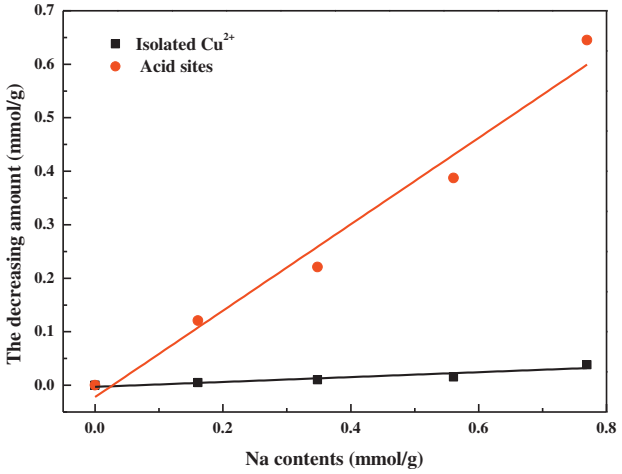

Fig. 9 – Decrease of acid sites (based on the results of NH_3-TPD) and isolated Cu^{2+} (based on the results of EPR) as a function of Na molar content.

2.3. NH_3-SCR reactions over Cu/SAPO-34

To understand how Na^+ affects the catalytic activity, the NH_3-SCR reaction was carried out and the results are shown in Fig. 8. Compared to Cu-F, the NO_x conversion of the Na-containing catalysts decreases. The NO conversion of the Na-containing catalysts declined with increasing Na^+ content. Notably, Cu-Na1.8 was the least active catalyst among all the samples.

Fig. 9 displays the results of kinetic experiments for all catalysts in the temperature range 170 to 230°C. The activation energies estimated from the Arrhenius plots show that all catalysts have a similar apparent activation energy (E_a = 39 ± 1.5 kJ/mol), which is reasonable compared with literature results (Wang et al., 2014, 2015a; Xue et al., 2013). The results also demonstrate that the presence of Na^+ does not change the reaction mechanism, rather it reduces the number of active sites.

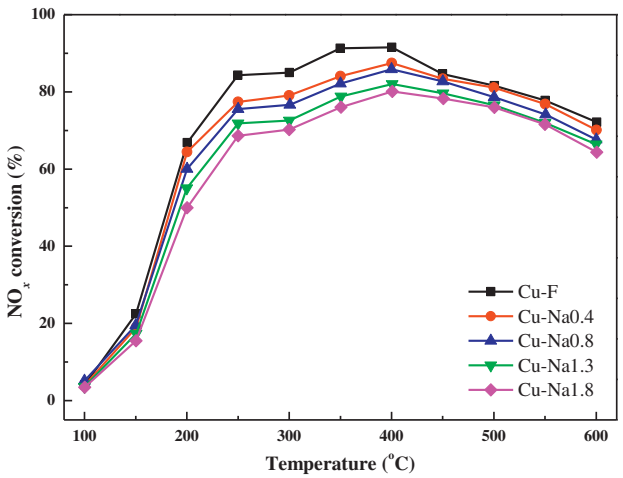

Fig. 8 – NH_3-SCR resluts of Cu/SAPO-34 catalysts. NH_3-SCR: ammonia selective catalytic reduction.

3. Discussion

3.1. Na effects on the structure and Cu species of Cu/SAPO-34

Our CO_2-DRIFTS results (Fig. 3) show that Si–O(Na^+)–Al structures exist on Na-containing samples. It reasonable to believe that Na^+ can exchange with H^+ or Cu^{2+} to form Si–O(Na^+)–Al. This assumption is supported by the NH_3-TPD and EPR results, which show that the amounts of acid sites and isolated Cu^{2+} decrease when Na^+ is introduced. The reduced numbers of acid sites (based on the results of NH_3-TPD) and isolated Cu^{2+} (based on the results of EPR) as a function of Na molar content were further considered and the results are shown in Fig. 9. The reduction in Brønsted acid sites (H^+) was much more pronounced than the reduction in isolated Cu^{2+}, which shows that Brønsted acid sites (H^+) are easily exchanged by Na^+. This is due to H^+ being more acidic than Cu^{2+}. After being exchanged by Na^+, the Cu^{2+} forms $CuAl_2O_4$-like species as corroborated by the H_2-TPR and EPR results. Similarly, H^+ is generated after the ion-exchange process, which helps to create a local acidic environment. As a result, the structure of Cu/SAPO-34 is slightly damaged. Since the extent of damage is negigible, the changes in acid and active sites are considered to be mainly caused by the ion exchange between Na^+ and H^+/Cu^{2+}. Based on the data we obtained above, a mechanism for Na^+ interaction with Cu/SAPO-34 can be proposed, as shown in Fig. 10.

3.2. Na effects on activity of Cu/SAPO-34

Fig. 8 shows that the NH_3-SCR activity of Cu/SAPO-34 decreases after Na introduction. Combining the effects of Na on the structure and on the Cu species of Cu/SAPO-34, the reasons for the activity loss of Cu/SAPO-34 after Na introducing are as follows:

Studies on the mechanism of NH_3-SCR suggest that the NH_3-SCR reaction over Cu/SAPO-34 includes two steps (Yu et al., 2014, 2015): the first step is the adsorption of NH_3 on

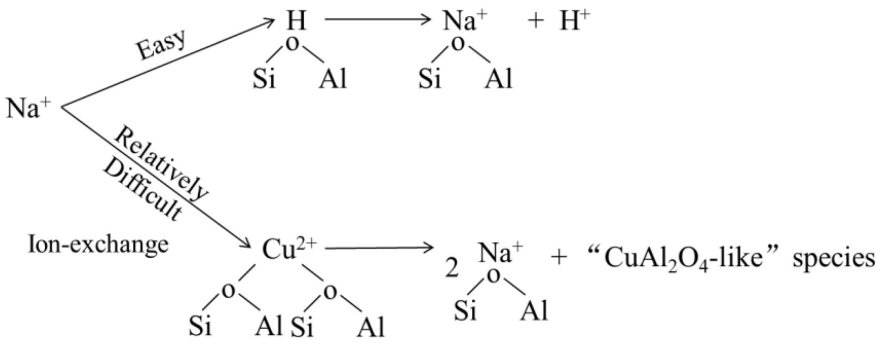

Fig. 10 – Sketch of the mechanism of Na interaction with Cu/SAPO-34.

Brønsted acid sites (H^+) and isolated Cu^{2+}, and the second step is reaction between the adsorbed NH_3 and NO. Since the SCR reaction only occurs on active isolated Cu^{2+}, NH_3 adsorbed on Brønsted acid sites (H^+) needs to migrate to isolated Cu^{2+} sites when reacting with NO. In the low temperature range (lower than 230°C), the migration rate is too slow, so NH_3 adsorbed on Brønsted acid sites (H^+) does not participate in the SCR reaction (Yu et al., 2015). Thus, the only factor affecting activity in this temperature range is the number of active isolated Cu^{2+} ions. To justify this assumption, the turnover frequencies (TOFs) were calculated and the data are shown in Fig. 11. TOFs, calculated based on the number of isolated Cu^{2+} ions measured by EPR, are identical for all samples. Therefore, the activity loss in this temperature range is attributed to the loss of isolated Cu^{2+} in the kinetically controlled temperature region.

At high temperatures (above 230°C), two reactions, NH_3-SCR and NH_3 oxidation, occur. NH_3 oxidation is considered to be the main side reaction, which has a negative effect on the high temperature NH_3-SCR activity. However, the influence of NH_3 oxidation is negligible in this study because the amount

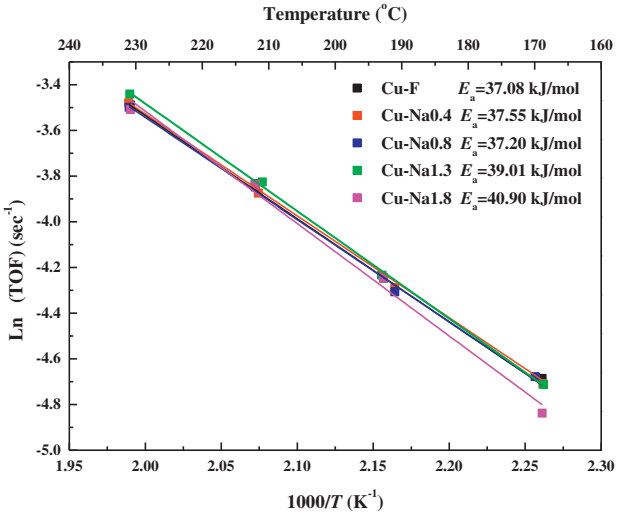

Fig. 11 – Ln (TOF) of NH_3-SCR reaction over Cu/SAPO-34 catalysts. TOF: turnover frequency; E_a: reaction activation energy; T: reaction temperature.

of CuO, which was proved to be the active site of NH_3 oxidation (Wang et al., 2014), remains the same for all samples. It has been reported that NH_3 migration from Brønsted acid sites to active Cu^{2+} sites is not the reaction rate determining step in NH_3-SCR at high temperatures (Duan et al., 2015; Yu et al., 2015). Thus, the effects of the NH_3 storage capacity on NH_3-SCR cannot be ignored (Wang et al., 2015b). The NH_3-TPD results show a drop in the NH_3 storage capacity of catalysts after Na introduction. Therefore, in addition to the loss of isolated Cu^{2+}, the loss of Brønsted acid sites is another reason for activity loss.

Our research probes the mechanism of the effect of Na^+ on Cu/SAPO-34. Similar to the K^+ effect, Na^+ causes activity loss by decreasing the number of active sites and acid sites on Cu/SAPO-34. However, the natures of the alkali metal effects on Cu/SAPO-34 are different from those on Cu/SSZ-13.

The different effects of alkali metal ions on Cu/SSZ-13 and Cu/SAPO-34 may relate to the different alkali metal ion loading methods and the difference in high temperature hydrothermal stability between these two kinds of catalysts. All studies on the effect of alkali metal ions on Cu/CHA have indicated that alkali metal ions can undergo ion-exchange with Cu/CHA. Two studies (Fedeyko and Chen, 2015; Gao et al., 2015a) used ion exchange to load alkali metal ions on Cu/SSZ-13, and Cu^{2+} was loaded after or together with the alkali metal ion loading. Therefore, the alkali metal ions only affect "H^+" instead of "Cu^{2+}". In addition, Cu/SSZ-13 shows relatively poor hydrothermal stability compared with Cu/SAPO-34. The presence of Na^+ on Brønsted acid sites can mitigate the hydrolysis process. Even though the decrease of Si–OH–Al may influence the high temperature activity of Cu/SSZ-13 in theory, its positive effects of mitigating hydrolysis seem to be more significant. Thus, alkali metal ions exhibit positive effects on Cu/SSZ-13. However, in our study, we impregnated sodium salt solutions on Cu/SAPO-34 and find that both "H^+" and active "Cu^{2+}" decline, and the decline further leads to the activity loss of Cu/SAPO-34. In a word, alkali metal ions have a negative effect on Cu/SAPO-34.

4. Conclusion

The effects of Na^+ on Cu/SAPO-34 were investigated in this work. The results demonstrate that Na^+ exchanges with

both H^+ and Cu^{2+} of Cu/SAPO-34. Na^+ mainly substitutes for H^+ in Si–OH–Al to form Si–O(Na^+)–Al and H^+, and also substitutes for isolated Cu^{2+} to form Si–O(Na^+)–Al and "$CuAl_2O_4$-like" species. The NH_3-SCR activity decreases with increasing Na content. For temperatures below 230°C, the loss of active isolated Cu^{2+} is the reason for the activity loss, whereas for temperatures higher than 230°C, the declines of both active isolated Cu^{2+} and acid sites contribute to the activity loss.

Acknowledgements

This work was financially supported by the National Key Research and Development program (No. 2017YFC0211302), the National Natural Science Foundation of China (No. 21676195) and the Science Fund of State Key Laboratory of Engine Reliability (No. skler-201714).The authors wish to thank the finical support from GM Global Research & Development (No. GAC1539).

Appendix A. Supplementary data

Supplementary data to this article can be found online at https://doi.org/10.1016/j.jes.2017.11.002.

REFERENCES

Bonelli, B., Civalleri, B., Fubini, B., Ugliengo, P., Otero Areán, C., Garrone, E., 2000. Experimental and quantum chemical studies on the adsorption of carbon dioxide on alkali-metal-exchanged ZSM-5 zeolites. J. Phys. Chem. B 104 (47), 10978–10988.

Duan, Y.F., Wang, J., Yu, T., Shen, M.Q., Wang, J.Q., 2015. The role and activity of various adsorbed ammonia species on Cu/SAPO-34 catalyst during passive-SCR process. RSC Adv. 5 (19), 14103–14113.

Fan, S.K., Xue, J.J., Yu, T., Fan, D.Q., Hao, T., Shen, M.Q., et al., 2013. The effect of synthesis methods on Cu species and active sites over Cu/SAPO-34 for NH_3-SCR reaction. Catal. Sci. Technol. 3 (9), 2357–2364.

Fedeyko, J.M., Chen, H.Y., 2015. Zeolite Catalyst Containing Metals Patent No. 20150078989A1.

Fickel, D.W., D'Addio, E., Lauterbach, J.A., Lobo, R.F., 2011. The ammonia selective catalytic reduction activity of copper-exchanged small-pore zeolites. Appl. Catal. B Environ. 102 (3-4), 441–448.

Gao, F., Walter, E.D., Burton, S.D., Washton, N.M., Kwak, J.H., Szanyi, J., et al., 2013. Synthesis and evaluation of Cu-SAPO-34 catalysts for NH_3-SCR. ACS Catal. 3, 2083–2093.

Gao, F., Walter, E.D., Washton, N.M., Szanyi, J., Peden, C.H.F., 2015a. Synthesis and evaluation of Cu/SAPO-34 catalysts for NH_3-SCR 2: solid-state ion exchange and one-pot synthesis. Appl. Catal. B Environ. 162, 501–514.

Gao, F., Wang, Y., Washton, N.M., Kollár, M., Szanyi, J., Peden, C.H. F., 2015b. Effects of alkali and alkaline earth cocations on the activity and hydrothermal stability of Cu/SSZ-13 NH_3–SCR catalysts. ACS Catal. 5 (11), 6780–6791.

Garrone, E., Bonelli, B., Lamberti, C., Civalleri, B., Rocchia, M., Roy, P., et al., 2002. Coupling of framework modes and adsorbate vibrations for CO_2 molecularly adsorbed on alkali ZSM-5 zeolites: mid- and far-infrared spectroscopy and ab initio modeling. J. Chem. Phys. 117 (22), 10274–10282.

Ishihara, T., Kagawa, M., Hadama, F., Nishiguchi, H., Ito, M., Takita, Y., 1997. Thermostable molecular sieves, silicoaluminophosphate (SAPO)-34, for the removal of NOX with C_3H_6 in the coexistence of O_2, H_2O, and SO_2. Ind. Eng. Chem. Res. 36 (1), 17–22.

Koebel, M., Elsener, M., Kleemann, M., 2000. Urea-SCR: a promising technique to reduce NO_x emissions from automotive diesel engines. Catal. Today 59 (3), 335–345.

Li, Z., Wang, D., Liu, Y., Kamasamudram, K., Li, J., Epling, W., 2014. SO_2 poisoning impact on the NH_3-SCR reaction over a commercial Cu-SAPO-34 SCR catalyst. Appl. Catal. B Environ. 156–157 (9), 371–377.

Liu, X.S., Wu, X.D., Weng, D., Si, Z.C., 2015. Durability of Cu/SAPO-34 catalyst for NO_x reduction by ammonia: potassium and sulfur poisoning. Catal. Commun. 59, 35–39.

Liu, J.X., Yu, F.H., Liu, J., Cui, L.F., Zhao, Z., Wei, Y.C., et al., 2016. Synthesis and kinetics investigation of meso-microporous Cu-SAPO-34 catalysts for the selective catalytic reduction of NO with ammonia. J. Environ. Sci. 48 (10), 45–58.

Ma, J., Si, Z.C., Weng, D., Wu, X.D., Ma, Y., 2015. Potassium poisoning on Cu-SAPO-34 catalyst for selective catalytic reduction of NO_x with ammonia. Chem. Eng. J. 267, 191–200.

Ma, J., Si, Z.C., Wu, X.D., Weng, D., Ma, Y., 2016. Optimizing the crystallinity and acidity of H-SAPO-34 by fluoride for synthesizing Cu/SAPO-34 NH3-SCR catalyst. J. Environ. Sci. 41 (3), 244–251.

Martínez-Franco, R., Moliner, M., Franch, C., Kustov, A., Corma, A., 2012. Rational direct synthesis methodology of very active and hydrothermally stable Cu-SAPO-34 molecular sieves for the SCR of NO_x. Appl. Catal. B Environ. 127 (17), 273–280.

Panahi, P.N., Niaei, A., Salari, D., Mousavi, S.M., Delahay, G., 2015. Ultrasound-assistant preparation of Cu/SAPO-34 nanocatalyst for selective catalytic reduction of NO by NH_3. J. Environ. Sci. 35 (9), 135–143.

Prakash, A.M., Unnikrishnan, 1994. Synthesis of SAPO-34: high silicon incorporation in the presence of morpholine as template. J. Chem. Soc. Faraday Trans. 90 (15), 2291–2296.

Shen, M.Q., Wen, H.Y., Hao, T., Yu, T., Fan, D.Q., Wang, J.Q., et al., 2015. Deactivation mechanism of SO_2 on Cu/SAPO-34 NH_3-SCR catalysts: structure and active Cu^{2+}. Catal. Sci. Technol. 5 (3), 1741–1749.

Wang, L., Li, W., Qi, G.X., Weng, D., 2012. Location and nature of Cu species in Cu/SAPO-34 for selective catalytic reduction of NO with NH_3. J. Catal. 289 (5), 21–29.

Wang, J., Liu, Z., Gang, F., Chang, L., Bao, W., 2013. In situ synthesis of CuSAPO-34/cordierite and its selective catalytic reduction of nitrogen oxides in vehicle exhaust: the effect of HF. Fuel 109 (11), 101–109.

Wang, J., Huang, Y., Yu, T., Zhu, S., Shen, M.Q., Li, W., et al., 2014. The migration of Cu species over Cu–SAPO-34 and its effect on NH_3 oxidation at high temperature. Catal. Sci. Technol. 4 (9), 3004–3012.

Wang, J., Fan, D.Q., Yu, T., Wang, J.Q., Hao, T., Hu, X.Q., et al., 2015a. Improvement of low-temperature hydrothermal stability of Cu/SAPO-34 catalysts by Cu^{2+} species. J. Catal. 322, 84–90.

Wang, L., Li, W., Schmieg, S.J., Weng, D., 2015b. Role of Bronsted acidity in NH_3 selective catalytic reduction reaction on Cu/SAPO-34 catalysts. J. Catal. 324 (1), 98–106.

Wondraczek, L., Gao, G., Möncke, D., Selvam, T., Kuhnt, A., Schwieger, W., et al., 2013. Thermal collapse of SAPO-34 molecular sieve towards a perfect glass. J. Non-Cryst. Solids 360 (1), 36–40.

Xie, L.J., Liu, F.D., Shi, X.Y., Xiao, F.S., He, H., 2015. Effects of post-treatment method and Na co-cation on the

hydrothermal stability of Cu–SSZ-13 catalyst for the selective catalytic reduction of NO_x with NH_3. Appl. Catal. B Environ. 179 (1), 206–212.

Xue, J.J., Wang, X.Q., Qi, G.X., Wang, J., Shen, M.Q., Li, W., 2013. Characterization of copper species over Cu/SAPO-34 in selective catalytic reduction of NO_x with ammonia: relationships between active Cu sites and de-NO_x performance at low temperature. J. Catal. 297 (1), 56–64.

Yu, T., Wang, J., Shen, M.Q., Li, W., 2013. NH_3-SCR over Cu/SAPO-34 catalysts with various acid contents and low Cu loading. Catal. Sci. Technol. 3 (12), 3234–3241.

Yu, T., Hao, T., Fan, D.Q., Wang, J., Shen, M.Q., Li, W., 2014. Recent NH_3-SCR mechanism research over Cu/SAPO-34 catalyst. J. Phys. Chem. C 118 (13), 6565–6575.

Yu, T., Wang, J., Qi, G.X., Li, W., Shen, M.Q., 2015. NH_3-SCR mechanism over Cu/SAPO-34 catalyst: the relation between reaction kinetic study of adsorbed ammonia species and saddle profile in NO conversion. Proceding of the North American Catalysis Society Meeting. Pittsburgh, America, June 14-19.